J. At. Mol. Sci.
doi: 10.4208/jams.090915.101215a

Vol. **6**, No. 4, pp. 272-282
November 2015

Dynamics of femtosecond pulsed laser induced Ti plasmas under different pressures

Dong Liu[a], Chuan-Song Chen[a], Xun Gao[b], Jing-Quan Lin[b], Bao-Yuan Man[a,*], Mei Liu[a,*], Yan-Na Sun[a], and Fei-Fei Li[a]

[a] *School of Physics and Electronics, Shandong Normal University, Jinan, 250014, the People's Republic of China*
[b] *School of Science, Changchun University of Science and Technology, Changchun, 130022, the People's Republic of China*

Received 9 September 2015; Accepted (in revised version) 12 October 2015
Published Online 15 November 2015

Abstract. The femtosecond laser ablation process and induced breakdown spectroscopy of transition metal Ti in air background has been investigated systematically. The ablation process is simulated by means of a three-dimensional two temperature model (3D-TTM). The time-resolved spectroscopy is employed to determine the characteristics of plasma during its evolution. The time-of-flight spectroscopy (TOFS) is also used to characterize the plasma expansion. The evolution behaviors of the plasma and its spectral characteristics have been analyzed as a function of pressure. It is shown that the component, expansion behavior and characteristics of the plasma have strong pressure dependences. The results are discussed in terms of the interaction mechanisms between ambient air and plasma species.

PACS: 32.30.Jc, 32.70.Jz

Key words: Femtosecond laser ablation; Two temperature model; Laser induced breakdown spectroscopy.

1 Introduction

Laser ablation is one of the basic physical phenomena when intense and ultrashort laser pulses interact with solid material. Meanwhile it is an important application of the laser-material interaction [1-2]. Due to the extremely high power density and ultrafast interaction with material, the femtosecond pulses are able to ablate the material without evident thermal effect and therefore act as a useful tool for micro-machining [3-4]. Meanwhile, the fs-laser ablation process is always companied by spectral emissions which was

*Corresponding author. *Email addresses:* byman@sdnu.edu.cn (B.-Y. Man)

called fs-laser induced breakdown spectroscopy (FLIBS) [5-6]. The laser induced breakdown spectroscopy (LIBS) can act as a potentially useful tool for numerous applications in material surface microanalysis and provide the information about the component of the sample surface [5]. Moreover, the FLIBS improves the spatial resolution and spectral sensitivity of the traditional LIBS analysis and can be applied in more delicate and complicate works [7-9], such as chemical mapping and depth profiling of complex biological systems [10-13].

With the evolutions of fs-laser induced plasma being generally understood, a more detailed and comprehensive understanding of Ti particles in fs-laser plasma is desired [14-16]. A sufficient understanding should include the component and evolution of the plasma. Particularly, the ambient gas plays an indispensable role in the behavior of the plasma characteristics. The collisions of the plasma species with the ambient gas will seriously impact the kinetic and optical properties of the laser plasma. Until now the phenomena due to the existence of ambient gas have been investigated widely, such as shielding effect, expanding velocity and laser supported detonation wave (LSDW) [8, 16]. However, there are few reports about the pressure effect on the dynamics of the fs-laser induced Ti plasma as far as we know.

In addition, investigation on the fs-laser ablation can serve to evaluate the early stage of the plasma formation [17-19]. This non-equilibrium heating process is generally described by the two temperature heat-conduction model (TTM) [20-21]. The theoretical simulations based on TTM are able to provide the temporal temperature behavior of the target and therefore give the information about the timescale of material removal and the early formation of plasma.

In present work, the fs-laser ablation of Ti target and the induced plasma have been investigated systematically. The ablation process is simulated by a three-dimensional two temperature model (3D-TTM) and the onset point of the material removal from the Ti surface is evaluated. The particular attention has been paid on the pressure effect on plasma evolution. The detailed informations about the plume species and expanding velocities are achieved and analyzed by time-resolved spectra and time-of-flight profiles. The pressure dependences of these properties are discussed in detail. The theoretical and experimental studies shown in this article will contribute to an insight into the characteristics of fs-laser plasma.

2 Experimental method

The experimental investigation of the plasma emission spectrum is implemented in the systems as shown in Fig. 1. An optical amplifier system (Hidra 25) generating 1000 fs laser pulses is used as the excitation source. The wavelength of the laser pulse is 800nm. A titanium plate (20 mm $\times$ 20 mm $\times$ 2 mm) with the purity of 99.999% is adopted as the sample. The laser beam is focused on the sample surface with the diameter of $\sim$200 μm in a vacuum chamber. The pressure is changed from 10Pa to 1atm. The peak power

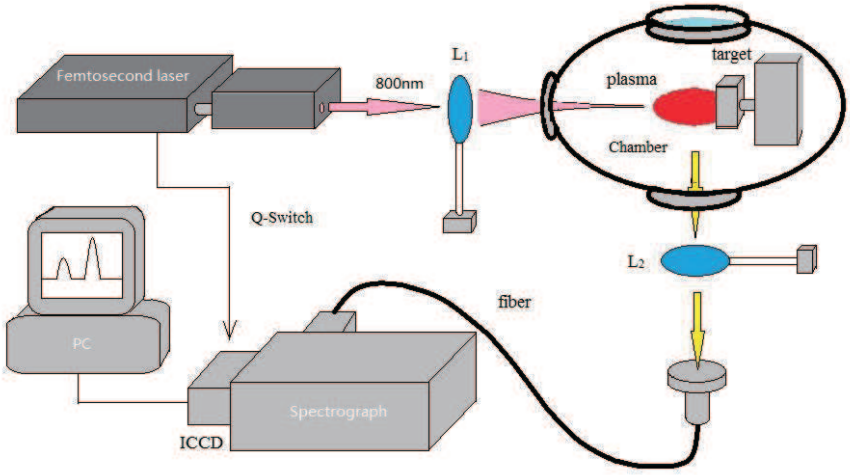

Figure 1: Experimental setup.

density on the titanium surface reaches as high as $2.17 \times 10^{14} W/cm$. The sample is fixed on a mobile platform in order to make sure that each laser shot ablates different spot on the sample surface.

The plume spectrum is coupled into an optical fiber probe which is connected to a grating spectrometer (Spectra Pro500i). As the means of detection, the spectrometer has been equipped with an intensified charge coupled device (PI MAXII ICCD). The pulses are operated at a 1 kHz repetition rate and a Q-switch signal is delivered to the ICCD to trigger the data acquisition gate when each pulse is generated. The spectra are acquired with a 10 ns gate width. The time delay between the laser pulse and acquisition gate is controlled by a pulse trigger generator (PTG). The spectral resolution of the system is 0.05 nm.

3 Formation of plasma

3.1 Theoretical methods

In order to describe the ultrafast material removal under fs-laser treatment, a three dimensional two temperature model (3D-TTM) is employed to simulate the evolution of the temperatures of electron and lattice near the target surface. The model is composed of two coupled nonlinear differential equations.

$$C_e \frac{\partial T_e}{\partial t} = K_e\left(\frac{\partial^2}{\partial r^2} + \frac{1}{r}\frac{\partial}{\partial r} + \frac{\partial^2}{\partial z^2}\right)T_e - g(T_e - T_l) + S(r,z,\theta,t); \tag{1}$$

$$C_l \frac{\partial T_l}{\partial t} = g(T_e - T_l). \tag{2}$$

Table 1: The major physical properties of Ti, including atomic mass m_A, optical absorption coefficient at 800nm α, specific mass ρ, specific heat C_l, thermal conductivity k_0, and thermodynamic equilibrium critical temperature T_{tc}.

	m_A(amu)	$\alpha(10^8/\mathrm{m})$	$\rho(10^3\mathrm{kg/m^3})$	C_l(J/kg·K)	k_0(W/m·K)	T_{tc}(K)
Ti	47.9	0.6	4.51	523	22	4623

The Gaussian laser source item is written as follow:

$$S(r,z,\theta,t) = I_0(1-R)\alpha\exp[-2r^2/\omega_0^2-(t-\tau)^2/2\tau^2-\alpha z]. \tag{3}$$

Where T_e and T_l are electron and lattice temperatures, respectively; C_e and C_l are the electronic and lattice heat capacities. K_e is the electron thermal conductivity which varies with the electron temperature in the form of $K_e = K_0 T_e/T_l$ [20-22]; g is electron-phonon coupling coefficient. The laser parameter τ denotes the pulse length, I_0 indicates the peak power density and ω_0 represents the radius of the laser spot. In addition, R denotes the optical reflectivity of the material surface and α indicates the optical absorption coefficient of Ti at the wavelength of 800nm. The TTM equation set is established in a cylindrical coordinate system with the radius r, the included angle θ between r and the x-axis, and the ablating depth z.

The thermodynamic parameters C_e and g are strongly temperature dependent for Ti. Here, we evaluate the two parameters with the method in Ref. [22,23]. Other physical parameters of Ti are presented in Table 1 [19, 24-27].

Considering the initial target temperature being set to be 300 K, the initial conditions and the boundary conditions can be described as:

$$T_e(r,z,\theta,0) = T_l(r,z,\theta,0) = T_0 \tag{4}$$

$$\left[\frac{\partial T_e(r,z,\theta,t)}{\partial r}+\frac{\partial T_e(r,z,\theta,t)}{\partial z}\right]\Bigg|_{r=R_0} = \left[\frac{\partial T_e(r,z,\theta,t)}{\partial r}+\frac{\partial T_e(r,z,\theta,t)}{\partial z}\right]\Bigg|_{z=0,d_0} = 0 \tag{5}$$

$$\left[\frac{\partial T_l(r,z,\theta,t)}{\partial r}+\frac{\partial T_l(r,z,\theta,t)}{\partial z}\right]\Bigg|_{r=R_0} = \left[\frac{\partial T_l(r,z,\theta,t)}{\partial r}+\frac{\partial T_l(r,z,\theta,t)}{\partial z}\right]\Bigg|_{z=0,d_0} = 0 \tag{6}$$

where T_0 denotes the room temperature. R_0 and d_0 denote the maximum simulated radius and depthArespectively. The equations are solved by the high resolution finite difference time-domain method (HR-FDTD) in FORTRAN 4.0 compiler. Thus the evolution of electron and lattice temperatures with the time will be achieved.

3.2 Ablation of target

Generally, the mechanisms of the laser ablation include intensive thermal evaporation, phase explosion, hydrodynamic sputtering, spallation, laser-induced charging and Coulomb explosion. The ablations based on different mechanisms take place simultaneously and are closely intertwined with each other [28]. The material removal is believed to be

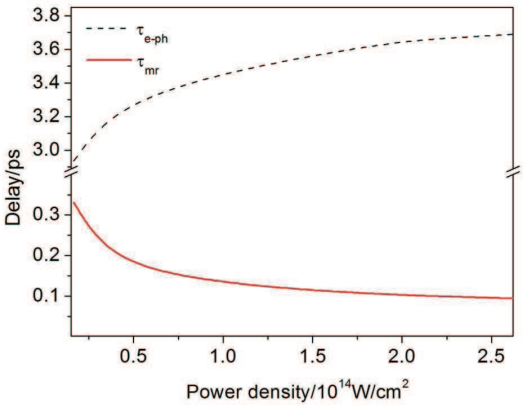

(a)

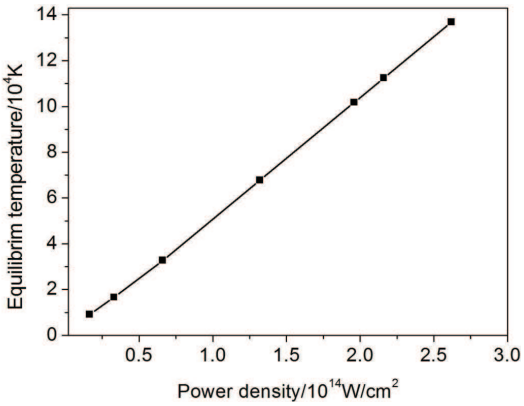

(b)

Figure 2: The variation of τ_{mr} and τ_{e-ph} (a) and the equilibrium temperature (b) as a function of laser power density.

mainly caused by phase explosion (PE) for the fs-ablation of metal at very high fluences as the report of Grojo and Hermann [19] .This can be also proved by the weak dependence of the plasma expanding velocity on laser power density, which will be discussed in the next section . A surface region ejects atoms or molecules and liquid droplets explosively when the target is superheated beyond the limit of thermodynamic stability of the target material. This process is named as phase explosion (PE). It is commonly assumed that the temperature threshold of PE is about 90% of the material critical temperature T_{tc} [15, 17, 28]. Therefore, the onset point of material removal can be defined as the time when the lattice temperature reaches T_{tc}.

It is convenient to define τ_{mr} as the onset time of the material removal, and τ_{e-ph} as electron-lattice relaxation time. The variation of the τ_{mr} and τ_{e-ph} with laser power density is illustrated in Fig. 2(a). The equilibrium temperature as a function of laser intensity is given in Fig. 2(b) which demonstrates a near linear dependence of the equilibrium

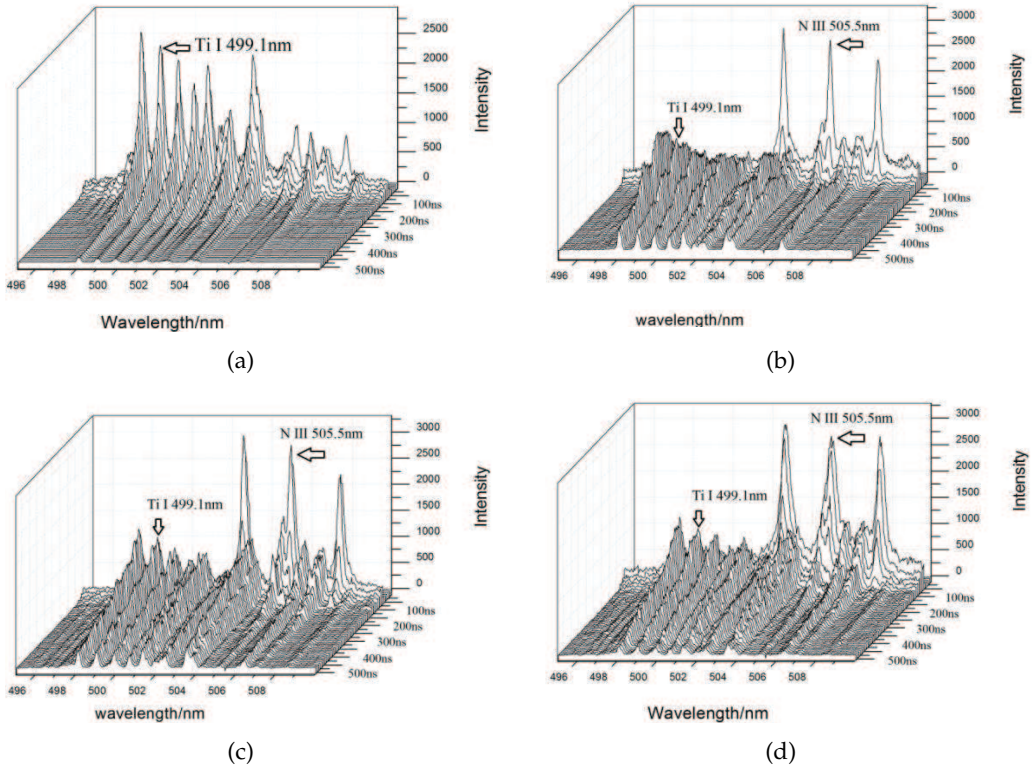

Figure 3: The evolution of spectral lines of different plasma species under different air pressures. (a)10 Pa, (b)100 Pa, (c)1000 Pa, (d)10000 Pa.

temperature on laser intensity. The material removal takes place in less than 1ps after the laser pulse with the laser power densities in the range of $0.3 \times 10^{14} W/cm^2$ to $2.6 \times 10^{14} W/cm^2$ as indicated by the solid curve in Fig 2(a). On the other hand, the thermal equilibrium between electron and lattice sub-systems has been attained in several picoseconds, as denoted by the dot curve.

For the power density $2.17 \times 10^{14} W/cm^2$ in the present experiment, the onset of material removal for Ti target is about 100fs. The result can be deduced that the excitation and ionization of N would take place less than 100 fs. The reason is that the primary mechanism of Ti removal is PE mentioned above which takes place only when the target surface is superheated to near 0.9 T_{tc}, while the nitrogen atoms are ionized directly by multiphoton-ionization (MI) under fs-laser pulse, which must be much faster. The ambient gas will absorb energy from the trailing edge of laser pulse. Consequently, the fs-ablation induced the shielding effect of air, which can be proved by the emission behavior of plasma as shown in Fig. 3. The effect will be discussed in detail in the next section.

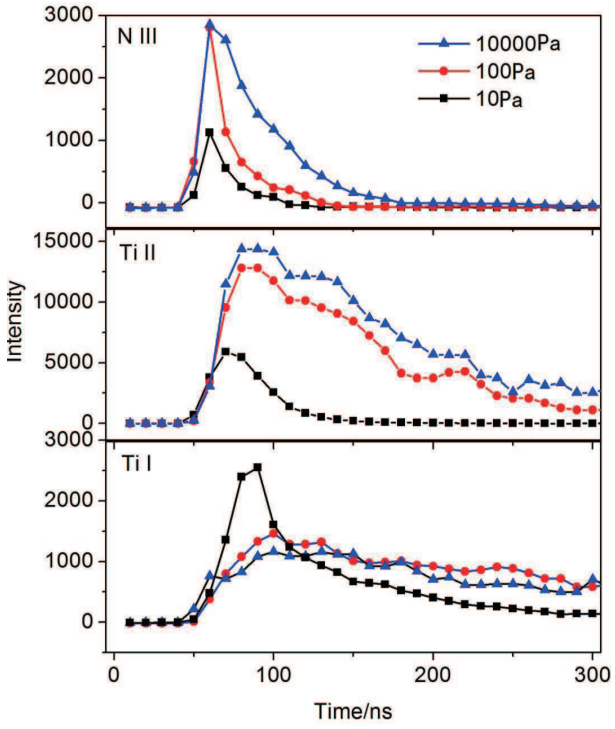

Figure 4: The line kinetics of the neutral and ionized species of metal and ambient air plasma under different pressures. (a) N III 505.5nm, (b) Ti II 375.9nm and (c) Ti I 498.1nm.

4 Analysis of spectrum

4.1 Plasma component and evolution

Spectral emissions from different species are radiated during the expansion of the plasma. The spectra are acquired at different ambient pressures (donated by p_0) ranging from 10 Pa to 1 atm. Fig. 3 shows the evolution of spectral lines from 495 nm to 510 nm where the emission spectra are dominated by spectral lines of Ti atoms and multicharged NIII ions with the laser power density $I_0 = 2.17 \times 10^{14} W/cm$. It is revealed that the continuum emission is weak under all pressures and almost absent under pressure of 10 Pa. The mean free path of vapor species within 10 Pa is larger than higher pressure [19]. Thus the collision probability of electrons with Ti atoms and ambient gas are smaller than that at higher pressure, which results in a weaker Bremsstrahlung emission, the primary mechanism of the continuum emission. Therefore, the continuum emission is suppressed, and a very high intensity ratio of characteristic lines and background emissions is demonstrated.

The atomic lines of Ti begin to rise over the continuum at the delay time of 50 ns. The inelastic collisions of electrons with Ti atoms and recombination of Ti ions result in a growing population of Ti atoms in excited levels ($3d^3 4p(^5G_6^0)$, $3d^3 4p(^5G_5^0)$, $3d^3 4p(^5G_3^0)$,

$3d^24s4p(^3D_1^0)$ and $3d^24s4p(^3D_3^0)$). The transitions from these levels to lower levels ($3d^34s(^5F_5)$, $3d^34s(^5F_4)$, $3d^34s(^5F_2)$, $3d^24s^2(^3F_2)$ and $3d^24s^2(^3F_4)$) are enhanced, which leads to a rise of corresponding lines (Ti I 498.1 nm, Ti I 499.1 nm, Ti I 500.7 nm, Ti I 501.4 nm and Ti I 506.4 nm). The atomic lines reach the peak intensities at the delay time more or less 100ns. After that, the plasma expansion and the heat diffusion from the plasma species to ambient air lead to the reduction of the emission intensities of spectral lines.

The emission evolutions of different plasma species indicated in Fig. 4 illustrate the line kinetics of the neutral and ionized species of metal and ambient gas (air) plasma (Ti I 498.1 nm, Ti II 375.9 nm and N III 505.5 nm lines) at different pressures. The upper levels of Ti II 375.9 nm ($3d^24p(^2F_{7/2}^0)$) and Ti I 498.1 nm ($3d^34p(^5G_6^0)$) lines are very close.

Fig. 4 shows that the emission of high ionized nitrogen ions (N III 505.5nm) is detected at about , and quickly reaches its maximum intensity. Then fast recombination of N ions because the high ionization potential leads to a rapid decay of N III line. The ionic line of Ti (Ti II 375.9 nm) starts to rise rapidly at the delay about 50 nsand approaches its maximum at 70 ns. The neutral emission (Ti I 498.1 nm) also appears at almost the same time. But the intensity of atomic line is much lower than that of ionic line due to the high ionization rate of Ti atoms in this time gap. After that, the recombination process of ions results in a fast decline of the ionic line. The process supplements the excited Ti atoms simultaneously and therefore leads to a slower decay of the Ti I line [29].

On the other hand, the evolution of Ti I line is much faster under p_0=10 Pa compared with higher pressure due to the fast expanding velocity of plasma. The weakness of N III line implies the air ionization is not significant for such a low pressure. However, the N III line is enhanced greatly while the intensity of Ti I line is seriously suppressed as pressure increases from 100 Pa to 10000 Pa. Moreover, the appearance of N III line suggests a very high ionization rate of the air. The intense air plasma will shield the Ti surface from the laser irradiation and therefore suppresses the excitation of Ti atoms.

It is worth noticed that the peak intensity ratio between Ti II 375.9 nm and Ti I 498.1 nm lines approaches 2.3 with p_0=10Pa, while the value increases to more than 10 with p_0=100Pa and to 14 with p_0=10000Pa, which is obtained in the Fig. 4. It indicates that in a higher pressure, the more excited atoms are ionized in the initial region.

Finally, the decay of all plasma species spectral intensities is slower at a higher pressure. The confinement effect of ambient air reduces the energy loss of the Ti plasma from expansion and therefore sustains the high intensity of the spectral lines for a longer time. Actually, the expanding velocity of the plasma is much slower at higher pressure as discussed in the following section, which can confirm the existence of the confinement effect.

4.2 Plasma expansion

The plasma expansion is analyzed by time-of-flight spectroscopy (TOFS) of neutral atoms. We define Z axis and R axis which represent axial direction and radial directions of the plume, respectively. The TOFS of Ti I 499.1 nm line along the two directions at the pres-

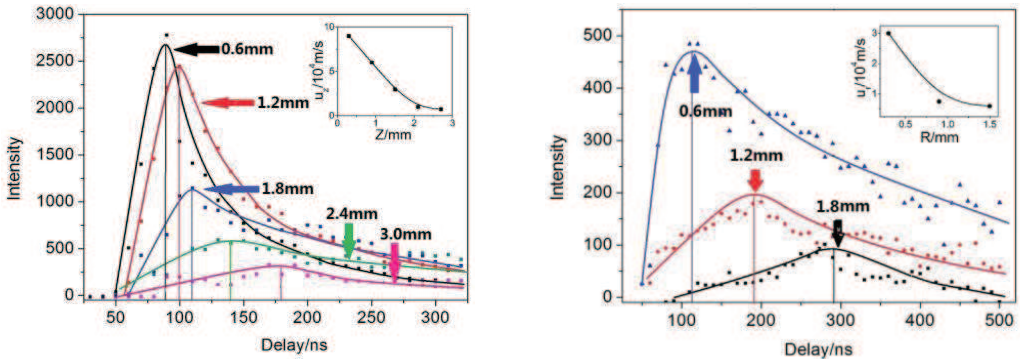

Figure 5: TOFS of Ti I 499.1nm line along Z (a) and R (b) directions of the plume. The variation of the expanding velocity along each axis is illustrated in top right corner.

sure p_0=10 Pa and laser intensity $I_0 = 2.17 \times 10^{14} W/cm^2$ is given in Fig. 5 (a) and (b), respectively. The variation of the expanding velocity along each axis is illustrated in top right corner of Fig. 5 (a). The TOFS indicates that the expanding velocity along Z axis u_z decreases with increasing Z. The velocity along R axis u_r also diminishes as a function of R. The internal pressure of the plasma vapor will drop with its expansion. So the expanding velocity will reduce owing to the combined action of the lowing pressure and the air confinement [30-32].

The two expanding velocities are measured as a function of pressure based on TOFS as illustrated in Fig. 6(a). The plasma expanding is slowed by higher pressure due to the more pronounced confinement effect. The significant air shielding effect under high pressure which leads to a attenuation of the laser intensity arriving at the target surface should also contribute to the reduction of the expanding velocity.

Fig. 6(b) illustrates the two velocities of Ti atoms at different laser intensity under p_0=10Pa. The weak dependence of the velocity on laser intensity allows to exclude the ablation mechanisms related to electrostatic phenomenon including space charge acceleration [33] and Coulomb explosion [34]. Because in that case, the change of the electric field associated with the laser intensity will alter the acceleration of the charged particles and vary the kinetic energies and therefore the expanding velocity.

5 Conclusion

The ablation process and the generated plasma of Ti led by 800 nm fs-laser have been investigated systematically by means of 3D-TTM theoretical method, time- resolved spectrum and time-of-flight profiles of plasma species. The ambient pressure dependence of the plasma evolution has been paid special attentions.

The results of 3D-TTM simulation show that the material removal of Ti target starts at a hundred femtoseconds after the laser pulse, while the MI of N should take place earlier

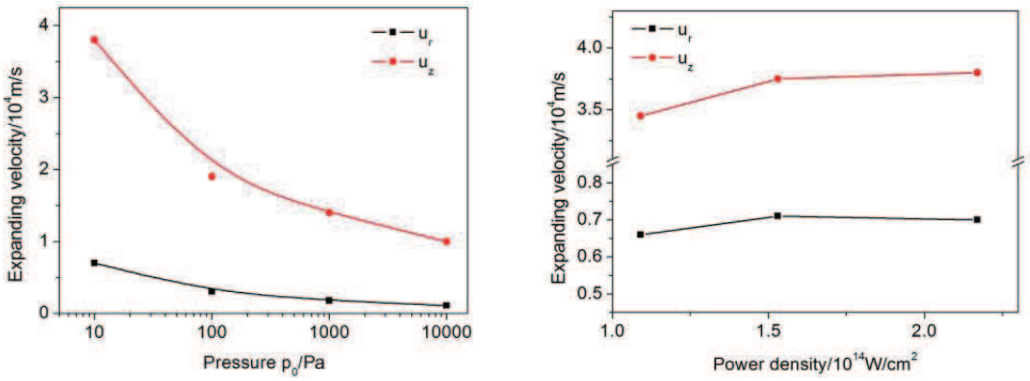

(a) (b)

Figure 6: Expanding velocities of the plume in axial and radial directions as a function of pressure (a) and laser power density (b).

and result in an absorption of the laser trailing edge. The time-resolved spectroscopy demonstrates that the N lines increases rapidly as a function of pressure while the Ti lines drops remarkably. Both of the above results have proved the existence of shielding effect of air for fs-laser ablation.

The time-resolved spectrum reveals that peak intensity ratio between Ti I lines and Ti II lines grows with pressure, which should be attributed to the increased ionization rate of Ti atoms. Moreover, the spectral lines of all plasma species evolve longer at a higher pressure due to the more pronounced confinement effect.

TOFS analysis of the Ti atomic line has been performed to determine the expanding velocity of the plume. The internal pressure of the plasma vapor will drop with its expansion. So the expanding velocity will reduce as a function of Z and R owing to the combined action of the lowing internal pressure and the air confinement. The expanding velocity also diminishes as a function of pressure, which should be caused by a more obvious confinement effect. A weak dependence of the expanding velocity on laser power density excludes the ablation mechanisms related to electrostatic phenomenon including space charge acceleration and Coulomb explosion.

The investigation contributes to an insight into the dynamics of evolution of fs-laser induced Ti plasma and should be meaningful for the analysis and applications of FLIBS.

Acknowledgments. This work is financially supported by the National Natural Science Foundations of China (Nos.11274204 and 11474187).

References

[1] Thorstensen, J.; Fosse, S. E. J. Appl. Phys. 2012, 112, 103514:1-11.
[2] Yang, J.; Zhao, Y.; Zhu, X. Appl. Phys. A 2007, 89, 571-578.
[3] Nolte, S.; Momma, C.; Jakobs, H.; Tunnermann, A.; Chichkov, B. N.; Wellegehausen, B.; Welling, H. J. Opt. Soc. Am. B 1997, 14, 2716-2722.

[4] Liu, X.; Du, D.; Mourou, G. IEEE Journal of Quantum Electronics, 1997, 33 (10), 1706-1716.
[5] Banerjee, S. P.; Chen, Z.; Fedosejevs, R. Optics and Lasers in Engineering 2015, 68A1-6.
[6] Noll, R. Laser-induced breakdown spectroscopy. Springer Berlin Heidelberg, 2012.
[7] Kaiser, J.; Novotny, K.; Martin, M. Z.; Hrdlicka, A.; Malina, R.; Hartl, M.; Adam, V.; Kizek, R. Surf. Sci. Rep. 2012, 67, 233-243.
[8] Dausinger, F.; Lichtner, F.; Lubatschowski, H. Femtosecond technology for technical and medical applications. Springer Science & Business Media, 2004.
[9] Jr. S. D.; Nunes, L. C.; Carvalho, G. G. A.; Gomes, M S.; Souza, P. F.; Leme, F. O.; Santos, L. G. C.; Krug, F. J. Spectrochim. Acta B 2012, 71-72, 3-13.
[10] Assion, A.; Wollenhaupt, M.; Haag, L.; Mayorov, F.; Sarpe-Tudoran, C.; Winter, M.; Kutschera, U.; Baumert, T. Appl. Phys.B 2003, 77, 391-397.
[11] Pinon, V.; Mateo, M. P.; Nicolas, G. Appl. Spectros. Rev. 2013, 48, 357-383.
[12] Reingruber, H.; Schröttner, H.; Zankel, A. Imag. Microscopy 2011, 2, 35-37.
[13] Mildner, J.; Sarpe, C. Appl. Surf. Sci. 2014, 302, 291-298.
[14] Cremers, A. D.; Yueh, F. Y.; Singh, J. P.; Zhang, H. S. Laser-Induced Breakdown Spectroscopy, Elemental Analysis. John Wiley & Sons, Ltd, 2006.
[15] Giacomo, A. D.; Shakhatov, V. A.; Senesi, G. S. Appl. Surf. Sci. 2002, 186, 533-537.
[16] Giacomo, A. D. Spectrochim. Acta B 2003, 58, 71-83.
[17] Mao, S. S.; Mao, X. L.; Greif, R.; Russo, R. E. Appl. Surf. Sci. 1998, 127-129, 206-211.
[18] Christensen, B. H.; Vestentoft, K.; Balling, P. Appl. Surf. Sci. 2007, 253, 6347-6352.
[19] Grojo, D.; Hermann,J.; Perrone, A. J. Appl. Phys. 2005, 97, 063306:1-9.
[20] Yang, J.; Zhao, Y.; Zhu, X. Appl. Phys. A 2007, 89, 571-578.
[21] Fourrier, T.; Schrems, G.; Muhlberger, T.; Heitz, J.; Arnold, N.; Bauerle, D.; Mosbacher, M.; Boneberg, J.; Leiderer, P. Appl. Phys. A 2001, 72, 1-6.
[22] Byskov-Nielsen, J.; Savolainen, J. M.; Christensen, M. S.; Balling, P. Appl. Phys. A 2011, 103, 447-453.
[23] Lin, Z. B.; Lei, Z. G. Phys. Rev. B 2008, 77, 075133:1-17.
[24] Ordal, M. A.; Long, L. L.; Bell, R. J.; Bell, S. E.; Bell, R. R.; Alexander, R. W.; Ward, C. A. Appl. Opt. 1983, 22(7), 16265-16271.
[25] Majchrzak, E.; Poteralska, J. Scientific Research of the Institute of Mathematics and Computer Science 2010, 9, 99-108.
[26] Chen, A.; Jiang, Y. F.; Liu, H.; Jin, M. X.; Ding, D. J. Laser Infrared 2012, 42(8), 847-851.
[27] D. E. Gray, American institute of physics handbook, Third edition, 1972.
[28] Lei, L. V. Z. G.; Lin, Z. B.; Ivanov, D. S. J. Phys. Chem. C, 2009, 113, 11892-11906.
[29] Hermann, J.; Vivien, C.; Carricato, A. P.; Boulmer-Leborgne, C. Appl. Surf. Sci. 1998, 127-129, 645-649.
[30] Lagrange, J. F.; Hermann, J.; Wolfman, J.; Motret, O. J. Appl. Phys. 2014, 116, 133303:1-7.
[31] Lagrange, J. F.; Wolfman, J.; Motret, O. J. Appl. Phys. 2012, 111, 063301:1-5.
[32] Dyer, P. E.; Issa, A.; Key, P. H. Appl. Surf. Sci. 1990, 46, 89-95.
[33] Gamaly, E. G. A.; Rhode, V.; Luther-Davies, B.; Tikhonchuk, V. T. Phys. Plasmas 2002, 9, 949-957.
[34] Stoian, R.; Ashkenasi, D.; Rosenfeld, A.; Campbell, E. E. B. Phys. Rev. B 2000, 62, 13167-13173.